

## Optical properties of nitride-rich SiN<sub>x</sub> and its use in CMOS-compatible near-UV Bragg filter fabrication

Wolffenbuttel, Reinoud F.; Winship, Declan; Qin, Yutao; Gianchandani, Yogesh; Bilby, David; Visser, Jaco H.

**DOI**

[10.1016/j.omx.2024.100348](https://doi.org/10.1016/j.omx.2024.100348)

**Publication date**

2024

**Document Version**

Final published version

**Published in**

Optical Materials: X

**Citation (APA)**

Wolffenbuttel, R. F., Winship, D., Qin, Y., Gianchandani, Y., Bilby, D., & Visser, J. H. (2024). Optical properties of nitride-rich SiN<sub>x</sub> and its use in CMOS-compatible near-UV Bragg filter fabrication. *Optical Materials: X*, 24, Article 100348. <https://doi.org/10.1016/j.omx.2024.100348>

**Important note**

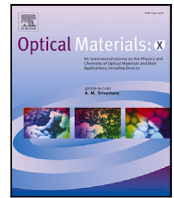
To cite this publication, please use the final published version (if applicable). Please check the document version above.

**Copyright**

Other than for strictly personal use, it is not permitted to download, forward or distribute the text or part of it, without the consent of the author(s) and/or copyright holder(s), unless the work is under an open content license such as Creative Commons.

**Takedown policy**

Please contact us and provide details if you believe this document breaches copyrights. We will remove access to the work immediately and investigate your claim.



## Optical properties of nitride-rich SiN<sub>x</sub> and its use in CMOS-compatible near-UV Bragg filter fabrication

Reinoud F. Wolffenbuttel<sup>a,\*</sup>, Declan Winship<sup>b</sup>, Yutao Qin<sup>b</sup>, Yogesh Gianchandani<sup>b</sup>, David Bilby<sup>c</sup>, Jaco H. Visser<sup>c</sup>

<sup>a</sup> Laboratory for Electronic Instrumentation, Department of Microelectronics, Delft University of Technology, 2628 CD Delft, The Netherlands

<sup>b</sup> Center for Wireless Integrated MicroSensing and Systems (WIMS2) and the Department of Electrical Engineering and Computer Science, University of Michigan, Ann Arbor, MI 48109, USA

<sup>c</sup> Research and Advanced Engineering, Ford Motor Company, Dearborn, MI 48121, USA

### ARTICLE INFO

#### Keywords:

Silicon-nitride  
Integrated silicon optical microsystems  
Near-UV optical filter  
Optical MEMS technology  
CMOS compatibility

### ABSTRACT

Nitride-rich silicon-nitride (SiN<sub>x</sub>) is being explored for its potential as a suitable optical material for use in microsystems operating in the near-UV spectral range. Although silicon-rich SiN<sub>x</sub> is widely accepted as a CMOS-compatible dielectric and micromechanical material, its optical absorption limits application to the visible to near-IR spectral range. However, this work shows that a balance can be achieved between a sufficiently high index of refraction ( $n > 2$ ) and an acceptable optical loss ( $k < 10^{-3}$ ) in nitride-rich SiN<sub>x</sub> of appropriate composition ( $x \sim 1.45$ ). Bragg reflectors with a design wavelength at  $\lambda_0 = 330$  nm are used for validation. PECVD is used for sample preparation and experiments confirm that the spectral range available for use of SiN<sub>x</sub>-based optical microsystems extends to wavelengths as low as 300 nm.

### 1. Introduction

#### 1.1. Background

Silicon-nitride (SiN<sub>x</sub>) is, next to silicon-dioxide (SiO<sub>2</sub>), one of the most commonly used materials in mainstream microelectronic fabrication for application as an insulating film [1,2]. Typically deposited by low-pressure chemical vapor deposition (LPCVD) or plasma-enhanced chemical vapor deposition (PECVD), SiN<sub>x</sub> is highly compatible with CMOS fabrication and is also used in micro-electro-mechanical system (MEMS) fabrication as a structural layer, because of its favorable mechanical properties such as the relatively high Young's modulus [3–5]. In a MEMS a slightly silicon-rich material composition ( $x < 4/3$ ) is generally preferred and deposited in such a way that the resulting layer is at slightly tensile stress to ensure that also double-side clamped suspended microstructures fabricated therein remain taut [5]. SiN<sub>x</sub> is also a suitable optical material and has found application in devices and microsystems ranging from a simple high-index optical layer to optical platforms for the visible and near-IR spectral range [6–9]. Such SiN<sub>x</sub>-based optical platforms are commercially available [10] and are offered as foundry product [11].

SiN<sub>x</sub> is a transparent dielectric with an optical bandgap varying with composition from about  $E_g = 2.6$  eV for highly Si-rich material, to  $E_g = 5.1$ – $5.3$  eV for the stoichiometric composition and up to  $E_g = 5.6$  eV

for N-rich material [12–14]. The Urbach energy is in the range 200–500 meV [15]. The optical properties of SiN<sub>x</sub> in the near-ultraviolet (near-UV) to near infrared (near-IR) spectral range are wavelength dependent and also depend on the material composition. At 633 nm wavelength the index of refraction,  $n$ , increases with silicon content and typical values range from  $n \sim 1.9$  for nitride-rich material ( $x > 4/3$ ), to  $n \sim 2$  for Si<sub>3</sub>N<sub>4</sub> (stoichiometric material,  $x = 4/3$ ) to  $n = 2.2$ – $2.3$  for silicon-rich material, while the extinction coefficient,  $k < 10^{-4}$  over the full range of practical compositions.

As shown in Fig. 1,  $n$  increases only slightly with decreasing wavelength over the near-IR to the short-wavelength visible (about +10% in the range from  $\lambda = 2$   $\mu\text{m}$  to  $\lambda = 500$  nm), while  $k$  remains very small. Their spectral dependency is much more pronounced in the near-UV, with  $n$  at  $\lambda < 450$  nm strongly increasing with decreasing wavelength [13,14]. Additionally, at a composition towards highly Si-rich material, a spectral peak that is due to its relatively small bandgap energy moves into the near-UV [4]. When using SiN<sub>x</sub> as the high-index material in optical filter design, a high value for  $n$  is desirable, thus favoring a Si-rich composition. However,  $k$  increases exponentially with decreasing wavelength and Si content in this spectral range, with  $k_{400\text{ nm}} > 0.1$  for the stoichiometric composition. As a result the associated optical loss renders a Si-rich material composition generally undesirable for an optical design intended for use in the near-UV.

\* Corresponding author.

E-mail address: [r.f.wolffenbuttel@tudelft.nl](mailto:r.f.wolffenbuttel@tudelft.nl) (R.F. Wolffenbuttel).

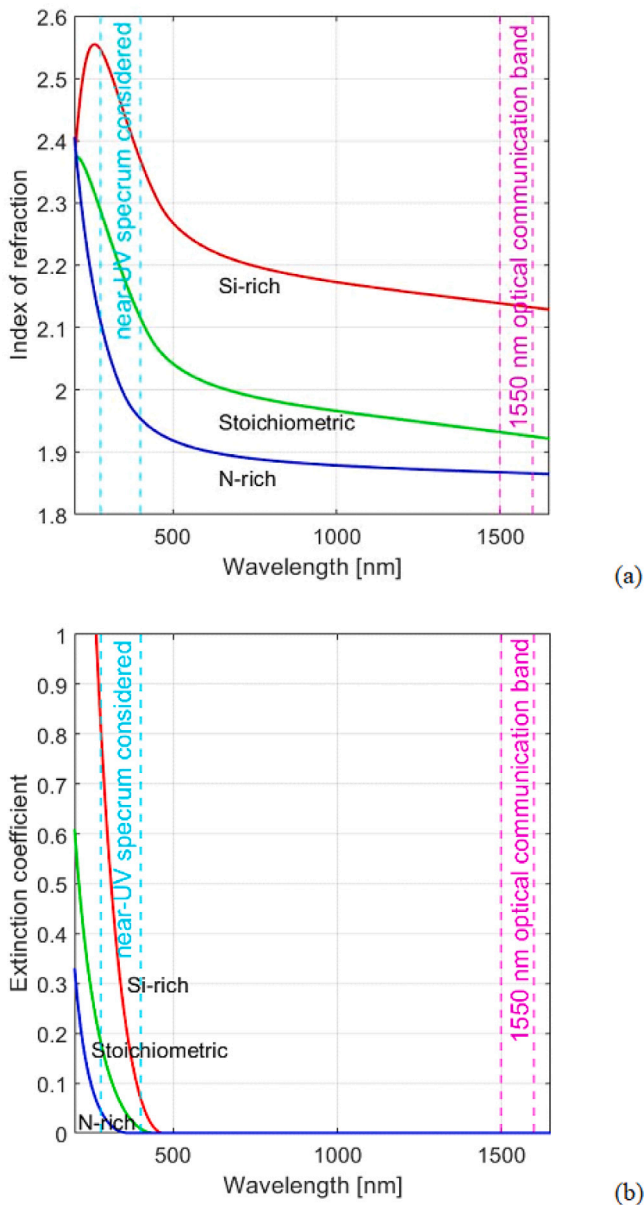


Fig. 1. Spectral dependencies of the index of refraction (a) and extinction coefficient (b) for  $\text{SiN}_x$  films of different composition.

The composition of a deposited  $\text{SiN}_x$  layer can be tuned by the flow settings of the precursor gases (usually (dichloro) silane and ammonia) and this dependency provides the opportunity for adapting the  $\text{SiN}_x$  optical properties to the requirements of the application considered. The composition,  $x$ , can in principle be controlled by the proportion of silane in the gas flow, which is denoted as  $R_g = \Phi_{\text{SiH}_4} / (\Phi_{\text{SiH}_4} + \Phi_{\text{NH}_3})$ , with  $\Phi_{\text{SiH}_4}$  the silane gas flow and  $\Phi_{\text{NH}_3}$  the ammonia gas flow. An increased  $\Phi_{\text{SiH}_4}$  results in an increased Si content in the layer deposited. As the index of refraction of Si in a Si-H bond is much higher as compared to that of N in a N-H bond, the overall index of refraction increases with Si content (thus with decreasing  $x$ ). However, the actual incorporation of atomic silicon from the silane flow into the material is not straightforward and is affected by mechanisms such as inclusion by hydrogenation. These effects have been extensively described in literature and are not further discussed here [1,14,16–20]. Although the repeatability of layer properties deposited by PECVD is generally believed to be more susceptible to hydrogenation effects as compared

to LPCVD, especially for N-rich  $\text{SiN}_x$ , PECVD is used here because of the lower temperature load on already integrated devices.

$\text{SiN}_x$ -on-Si devices are often planar waveguides with  $\text{SiN}_x$  serving as the waveguiding layer and  $\text{SiO}_2$  as the cladding. The Mach-Zehnder interferometer is usually implemented as the spectrally selective component in these devices. Systems that operate in the visible (630–660 nm band [7,9]) or in the near-IR (850 nm band or 1550 nm band [10,11]) have been reported, and mainly for optical communication. Vertical stacks of  $\text{SiN}_x$  and  $\text{SiO}_2$  layers on Si substrates have also been reported for reflective coating [21], anti-reflective coating in solar cell applications [16], or more generally for filtering in the near-IR spectral range, with a distributed Bragg reflector (DBR) providing the spectral selectivity. The DBR is basically composed of a stack of alternating dielectric layers of two different materials, with the one referred to as the high-index dielectric material ( $n_H$ ) and the other as the material of low-index ( $n_L$ ). The spectral selectivity of the DBR depends on the ratio between  $n_H$  and  $n_L$ , which is generally referred to as the index of refraction contrast,  $\Delta_c$ , and should be maximized [22]. In CMOS-compatible optical devices,  $\text{SiO}_2$  is usually the low-index material ( $n_L = 1.46$ – $1.51$ ), because of its very low optical loss over the entire near-UV, visible and near-IR spectral range.

The general challenge in optical MEMS design for the near-UV is the limited choice of suitable CMOS compatible high-index materials for fabrication of a DBR. The  $\text{TiO}_2/\text{SiO}_2$  combination, with  $\text{TiO}_2$  used as the material with  $n_H$  and  $\text{SiO}_2$  as the material with  $n_L$ , is often selected in a design for the visible spectrum [23,24]. The loss characteristics of the  $\text{TiO}_2$  make the material highly suitable in the visible spectral range, but generally not acceptable for use in the near-UV. In the 250–400 nm band,  $\text{HfO}_2$  is usually considered a very suitable candidate for  $n_H$  [25–27] and also  $\text{Ta}_2\text{O}_5$  is in principle applicable [28]. In these material combinations  $\text{SiO}_2$  remains the material of choice for  $n_L$ . Combinations of fluorides, such as  $\text{LaF}_3$  for  $n_H$  and  $\text{MgF}_2$  for  $n_L$ , can in principle also be considered, despite their limited CMOS fabrication compatibility, but their achievable  $\Delta_c$  is small [29–31]. A microspectrometer based on a linearly variable optical filter (LVOF), with  $\text{HfO}_2$  used as the high-index dielectric material ( $n_H$ ) and  $\text{SiO}_2$  as the material for the low-index ( $n_L$ ) layers, has been fabricated and successfully tested [32]. The stack of  $\text{HfO}_2$  and  $\text{SiO}_2$  layers was deposited by sputtering in a multiple-target sputter machine without breaking vacuum. However, sputtering is limited in the maximum thickness of layers that can be deposited in an efficient manufacturing process. This is one of the reasons for exploring the potential of PECVD  $\text{SiN}_x$  in this work.

When considering  $\text{SiN}_x$  as the high-index material in the near-IR, the compromise between a high refractive index and low optical loss can simply be skewed towards maximum refractive index. As material composition has a very minor adverse effect on  $k$  in the longer-wavelength visible and the near-IR, this can be accomplished by maximizing silicon-composition for achieving a high value of the index of refraction without a significant penalty in terms of optical loss. Other applications in optical sensors and waveguides for which the high-index property is particularly important are in silicon nanoparticles for use as light emitters in the visible range and in devices in which the Kerr effect is used for generating a non-linear optical effect in integrated silicon waveguides in the near-IR [14].

Because of the focus in literature on Si-rich  $\text{SiN}_x$  and its significant optical loss in the near-UV at such a composition, PECVD  $\text{SiN}_x$  for near-UV applications is often at forehand brushed aside, with few exceptions [21]. This is a pity, because the spectral response of a UV-enhanced photon detector in Si extends down to 200 nm. This property results from a careful design of the vertical doping profile of the junction in Si, combined with a special lateral design and backside illumination. The generic approach was already identified a long time ago [33], has evolved and subsequently has been adopted for CMOS imagers with an operating range down to the near-UV [34]. With few options available for adding optical functionality to such a UV-enhanced detector (array), the purpose of this work is to demonstrate the availability of a usable design window of N-rich  $\text{SiN}_x$  compositions for fabrication of optical microsystems operating in the near-UV.

**Table 1**  
Process parameters with  $\Phi_{NH_3} = 550$  sccm.

| Wafer type | Recipe           | $\Phi_{SiH_4}$ [sccm] | $R_g$ |
|------------|------------------|-----------------------|-------|
| A          | Slightly Si-Rich | 96                    | 0.149 |
| B          | Stoichiometric   | 84                    | 0.132 |
| C          | Slightly N-rich  | 70                    | 0.113 |
| D          | N-rich           | 45                    | 0.076 |

## 1.2. Specific aims and organization of the paper

Unlike the case of a near-IR design, tailoring the  $\text{SiN}_x$  for use in the near-UV requires a carefully tuned compromise for a composition that meets both the minimum index of refraction for a sufficiently high refractive index contrast, and the maximum of the extinction coefficient for an acceptable optical loss in the near-UV and thus a more subtle approach. The dependence of both the index of refraction and the optical loss on Si content in  $\text{SiN}_x$  is investigated. The material is deposited on prime Si wafers by PECVD with varying ratios of the silane and ammonia flow, such that  $\text{SiN}_x$  films are obtained with a composition in between slightly silicon-rich and nitride-rich ( $1.329 \leq x \leq 1.491$ ).

First, samples of PECVD  $\text{SiN}_x$  and  $\text{SiO}_2$  films are optically characterized by ellipsometry, followed by a preliminary analysis of their suitability as CMOS-compatible high-index optical material for use in the 250–400 nm band. Subsequently, three types of Bragg mirrors fabricated on Si wafers are analyzed (using MATLAB) for a design wavelength,  $\lambda_0 = 330$  nm. In these devices, the  $\text{SiN}_x$ , with a range of compositions from stoichiometric, slightly N-rich to N-rich, is used for the high-index layer, while  $\text{SiO}_2$  is used for the low-index layer. Finally, DBR designs are realized in a CMOS-compatible fabrication process and the experimentally obtained spectral responses are compared with simulations.

## 2. The optical properties of $\text{SiN}_x$

### 2.1. Measuring by ellipsometry and extracting $n$ and $k$

Table 1 shows four recipes that are evaluated in this work to assess the impact on composition and, eventually, on optical parameters. Note that the total gas flow is not kept constant between the different recipes. The deposition tool used is the GSI ULTRADEP 2000, which is a PECVD system operated at a temperature of 350 °C and is configured as a single chamber with a load-lock [35].

Samples of  $\text{SiN}_x$  layers of the four different compositions, each of about 40 nm thickness are deposited on 4" silicon wafers. Ellipsometry (Woollam M-2000) is used for characterization of film thickness and optical parameters  $n$  and  $k$  over the spectral range between 192 and 1686 nm, by using a measurement the complex spectral reflectance  $\rho = \tan(\Psi)e^{j\Delta}$  at three settings of the angle of incidence ( $\varphi = 55^\circ$ ,  $\varphi = 65^\circ$  and  $\varphi = 75^\circ$ ), with the parameter  $\Psi(\lambda, \varphi)$  used as a measure for the amplitude and  $\Delta(\lambda, \varphi)$  as a measure for the phase.

The layer thickness and wavelength dependent  $n(\lambda)$  and  $k(\lambda)$  are subsequently extracted from the ellipsometry data using a software tool CompleteEASE [36]. Extraction involves the use of a model for adjusting a dataset for  $n(\lambda)$  and  $k(\lambda)$  in such a way that the calculated spectral reflectance is a sufficiently close approximation of the measured set of  $\Psi(\lambda)$  and  $\Delta(\lambda)$  over the full spectral range and for all three angles of incidence. The Tauc-Lorentz (TL) and Cody-Lorentz (CL) models are generally used for that purpose [37]. While the CL model is dedicated to the extraction of the optical parameters near the band edge of amorphous semiconductors and is the best choice for analyzing, for instance, amorphous-Si thin films or SiC layers, the TL model is generally more suitable for extracting the optical parameters of dielectrics and semiconductors with low optical absorption below their bandgap [38–40].

**Table 2**  
Results of optical data extraction.

| Type | Recipe     | $\text{MSE}_{TL}$ | $\text{MSE}_{CL}$ | $n_{633}$ | $x_{impl}$ |
|------|------------|-------------------|-------------------|-----------|------------|
| A    | SI Si-rich | 1.93              | 1.84              | 2.023     | 1.932      |
| B    | Stoich.    | 3.10              | 2.24              | 2.012     | 1.343      |
| C    | SI N-rich  | 1.93              | 2.18              | 1.976     | 1.387      |
| D    | N-rich     | 3.83              | 4.25              | 1.896     | 1.491      |

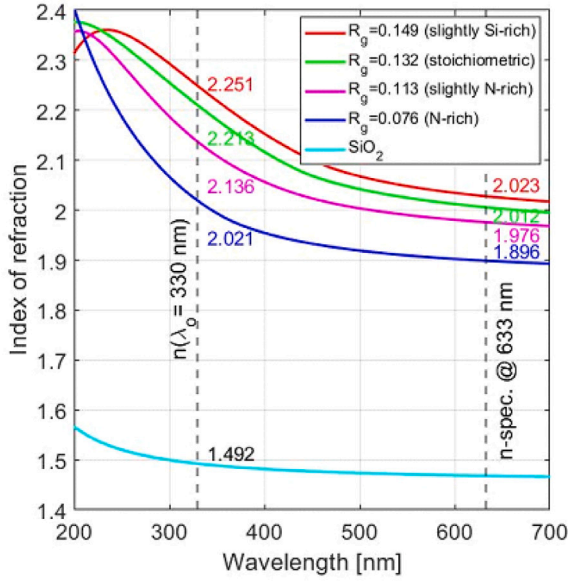
In the widely studied Si-rich  $\text{SiN}_x$  intended for use in the 1550 nm band (light of photon energy  $E_{ph} \sim 0.8$  eV, which is much smaller than the bandgap for any  $\text{SiN}_x$  composition) the TL model is generally considered the most appropriate, which is confirmed in literature on optical devices in  $\text{SiN}_x$  [14,16]. This argument is less persuasive in the near-UV. The 330 nm wavelength is considered here, which is associated with a significantly higher photon energy level,  $E_{ph} \sim 3.7$  eV. Moreover, this study has an emphasis on N-rich materials, with a bandgap energy  $E_g > 5.5$  eV and thus much larger as compared to  $E_g \sim 2.6$  eV for a Si-rich material. Both the TL and CL models have been tested and the results are shown in Table 2.

The MSE (Mean Squared Error) is used as a measure of the quality of the estimator. Although the MSE should be interpreted with care, a value in the range 2–5 is considered an indicator of a good fit and the model used is deemed appropriate, while an MSE larger than about 20 flags a poor fit and provides a warning that the model used is not very suitable. The data is subject to variation over the position on the wafer and the trend towards an increased MSE with  $x$ : the uncertainty  $\epsilon_{MSE} \sim \pm 2\%$  for measurement on the wafer coated with the stoichiometric composition (type B) and increases to  $\epsilon_{MSE} \sim \pm 6\%$  for the wafer coated with the N-rich film (type D). As a consequence, the least significant digit in the table listing only reflects the resolution used in the calculation and is not significant. The results do not provide conclusive evidence for a preferred use of the CL model for the extraction of  $n$  and  $k$  of  $\text{SiN}_x$  and it was decided to maintain compliance with literature and to use optical data extraction based on the TL model. Note that the table refers to the uncertainty in MSE and not to the variation in the extracted optical constants over the wafer, which is significantly smaller but not studied in detail. The results of TL data extraction are shown in Fig. 2. Although ellipsometry is performed over the full spectral range of the instrument (192–1686 nm), only the results over the wavelength range 200–700 nm are plotted.

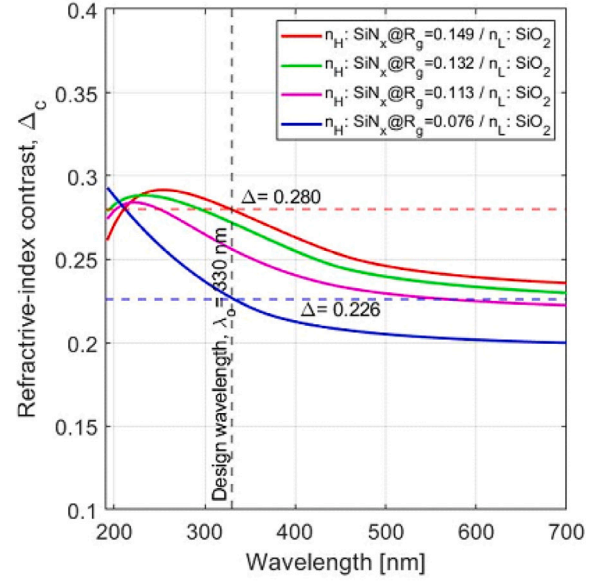
An empirical expression is available for deriving the material composition,  $x$ , from the measured (extracted) index of refraction,  $n_{meas}$ , relative to the index of refraction of each of the components in the composition of the material. This implied fraction  $x_{impl}$  is estimated from  $n_{meas}$  at 633 nm using [16–18]:

$$x_{impl} = \frac{[N]}{[Si]} = \frac{4}{3} \times \frac{n_{Si} - n_{meas}}{n_{Si} + n_{meas} - 2n_{Si_3N_4}} \quad (1)$$

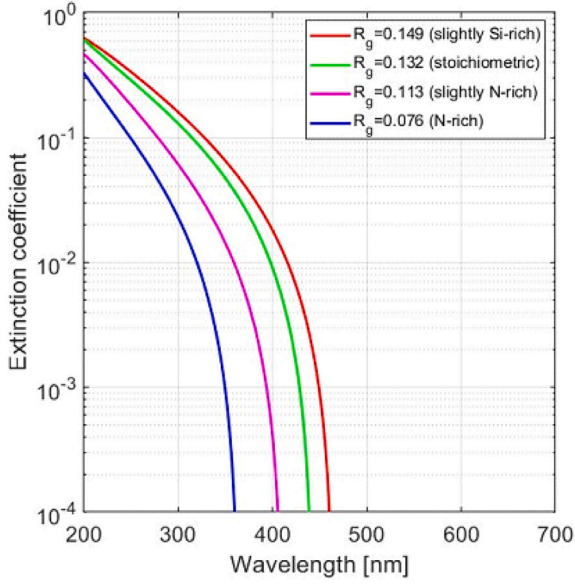
At the stoichiometric composition,  $x$  should be 4/3. The reference data on Si and  $\text{Si}_3\text{N}_4$  should be taken from samples that are deposited using the same type of technique, which is a highly relevant detail. While  $n_{Si}(633 \text{ nm}) = 3.88$  for crystalline (bulk) material, this value increases to  $n_{Si}(633 \text{ nm}) \sim 4.24$  in case of PECVD [16]. Similarly, for bulk material  $n_{Si_3N_4}(633 \text{ nm}) = 2.09$ . The consensus in literature on PECVD  $\text{SiN}_x$  is  $n_{Si_3N_4}(633 \text{ nm}) \sim 2.02$ , but a value as small as  $n_{Si_3N_4}(633 \text{ nm}) = 1.97$  is also reported [13,18]. Using these numbers and the data in Fig. 2 results in  $x_{impl}$  as listed in Table 2. The curves in Fig. 2 reveal that the distinguishing optical features of the material are in the shorter wavelength range, and the use of 633 nm as the reference wavelength is indeed criticized [41]. Although the films on wafers A and B can both be considered stoichiometric within the interval of uncertainty of the measurement, in this study only the recipes B, C and D are used for  $n_H$  in the optical design of test structures and that for  $\text{SiO}_2$  is used for  $n_L$ .



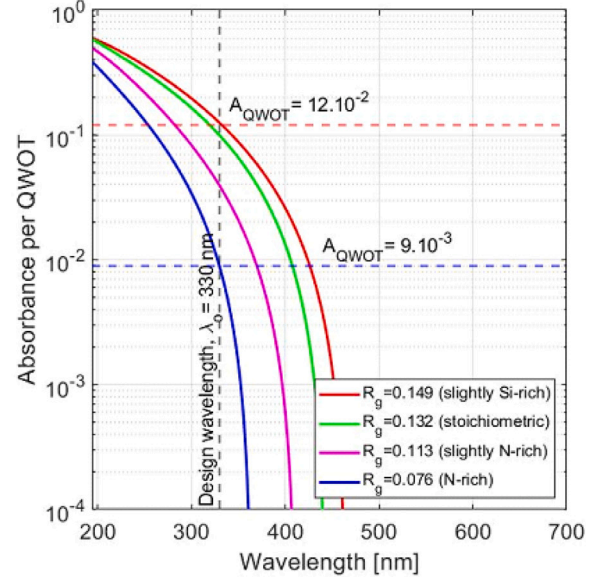
(a)



(a)



(b)



(b)

Fig. 2. Index of refraction (a) and extinction coefficient (b) for  $\text{SiN}_x$  films of different composition. These curves are extracted from ellipsometry data using the TL model. The data on  $\text{SiO}_2$  is extracted with the TL model with  $\text{MSE} = 2.12$ , while  $k_{\text{SiO}_2} < 10^{-4}$ .

Fig. 3. Derived performance parameters: (a) refractive index contrast,  $\Delta_c$ , and (b) absorbance per traversal through a QWOT layer,  $A_{\text{QWOT}}$ , for  $\text{SiN}_x$  films of different composition.

## 2.2. Using $\text{SiN}_x$ for the design of DBR's for the near-UV

The design of high-performance Bragg reflectors is extensively described in literature [22]. The main design parameter is the  $-3$  dB reflective bandwidth at the design bandwidth  $\lambda_o$ :

$$\frac{\Delta\lambda}{\lambda_o} = \frac{4}{\pi} \sin^{-1} \left( \frac{n_H - n_L}{n_H + n_L} \right) \quad (2)$$

This expression can be elaborated using the refractive index contrast,  $\Delta_c = (n_H^2 - n_L^2)/2n_H^2$ .

$$\frac{\Delta\lambda}{\lambda_o} = \frac{4}{\pi} \sin^{-1} \left( \frac{1 - \sqrt{1 - 2\Delta_c}}{1 + \sqrt{1 - 2\Delta_c}} \right) \quad (3)$$

Within the framework of this work a second performance parameter of equal importance is the absorbance per quarter-wavelength optical (layer) thickness (QWOT) section at  $\lambda_o$ ,  $t_{\text{QWOT}} = (4n(\lambda_o))^{-1}$ , which can

be expressed as:

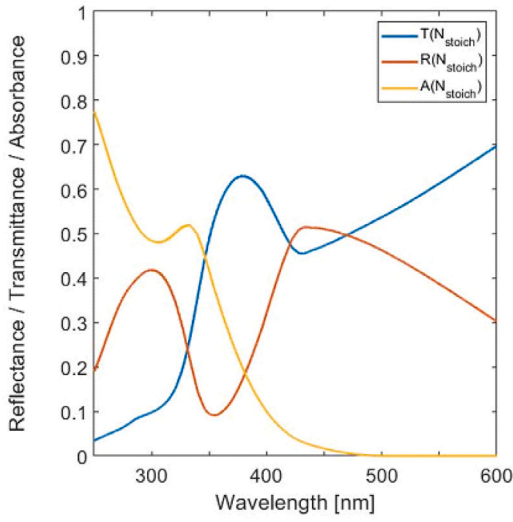
$$A_{\text{QWOT}} = e^{\alpha(\lambda)t_{\text{QWOT}}} = e^{-(4\pi k(\lambda)/\lambda) \times (\lambda/4n\lambda)} \quad (4)$$

with  $\alpha(\lambda) = 4\pi k(\lambda)/\lambda$  the spectral absorption coefficient of the material. Rewriting Eq. (4) results in:

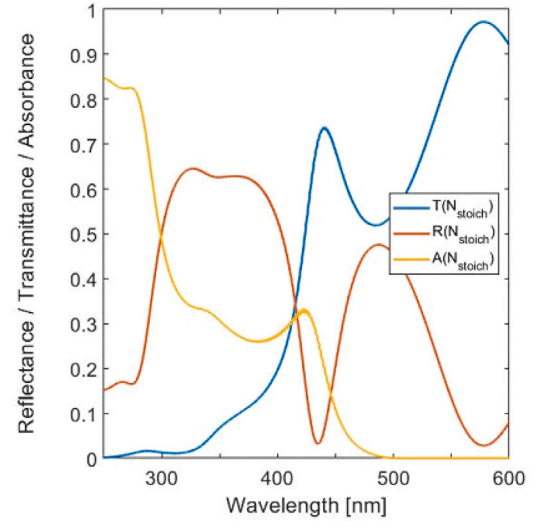
$$A_{\text{QWOT}} = e^{-\pi[k(\lambda)]/n(\lambda)} = [e^{-k(\lambda)}]^\pi/n(\lambda) \quad (5)$$

The last step in this derivation is particularly useful if the wavelength dependence of  $n$  is much less pronounced as compared to that of  $k$ . A constant  $n$  implies an exponential spectral dependence of  $A_{\text{QWOT}}$  on  $k$  only, which is in good approximation the case for  $\text{SiN}_x$  in the near-UV. Both  $\Delta_c$  and  $A_{\text{QWOT}}$  can be directly derived from the extracted optical properties. The results are shown in Fig. 3, which provides important clues with regard to the feasibility of a design.

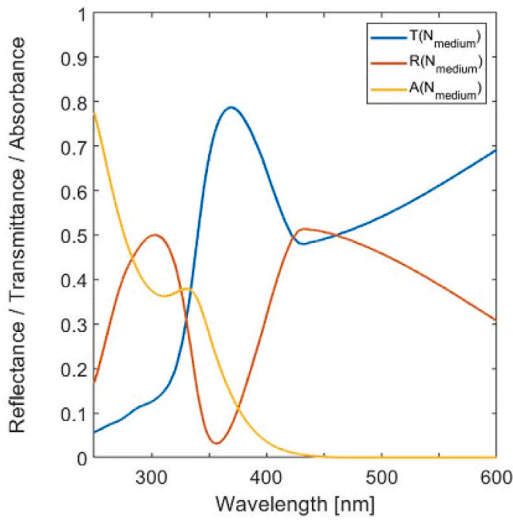
Only the N-rich material can be used if  $A_{\text{QWOT}}$  at the design wavelength of  $\lambda_o = 330$  nm needs to be limited to  $10^{-2}$ , while all material



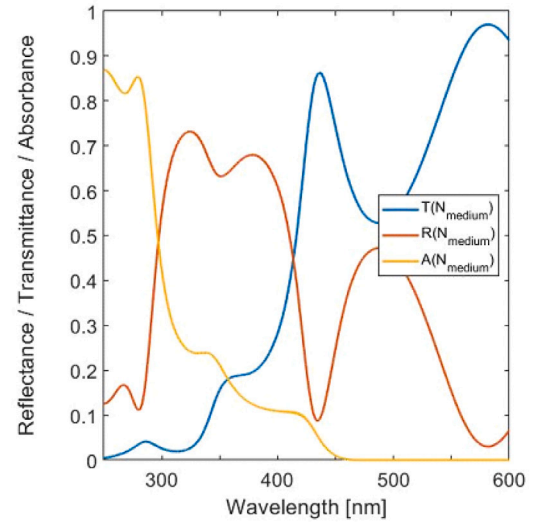
(a)



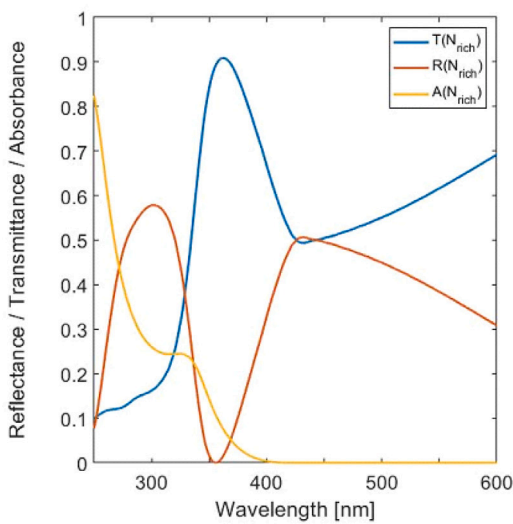
(a)



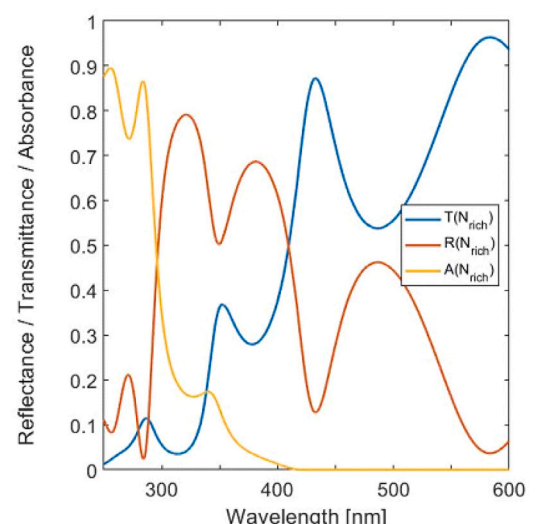
(b)



(b)



(c)



(c)

**Fig. 4.** Spectral reflectance, transmittance, and absorbance of the 3-layer H-L-H DBR on Si using layers of (a) 37.3 nm layer of  $\text{Si}_3\text{N}_4$  for  $n_H$ , (b) 38.6 nm of slightly N-rich  $\text{SiN}_x$  ( $N_{\text{medium}}$ ) for  $n_H$  and (c) 40.8 nm of N-rich  $\text{SiN}_x$  for  $n_H$ , each with layers of 55 nm of  $\text{SiO}_2$  for  $n_L$ .

**Fig. 5.** Spectral reflectance, transmittance, and absorbance of the 9-layer H-L-H-L-H-L-H-L-H-L-H DBR on Si using layers of (a) 37.3 nm layer of  $\text{Si}_3\text{N}_4$  for  $n_H$ , (b) 38.6 nm of slightly N-rich  $\text{SiN}_x$  ( $N_{\text{medium}}$ ) for  $n_H$  and (c) 40.8 nm of N-rich  $\text{SiN}_x$  for  $n_H$ , each with layers of 55 nm of  $\text{SiO}_2$  for  $n_L$ .

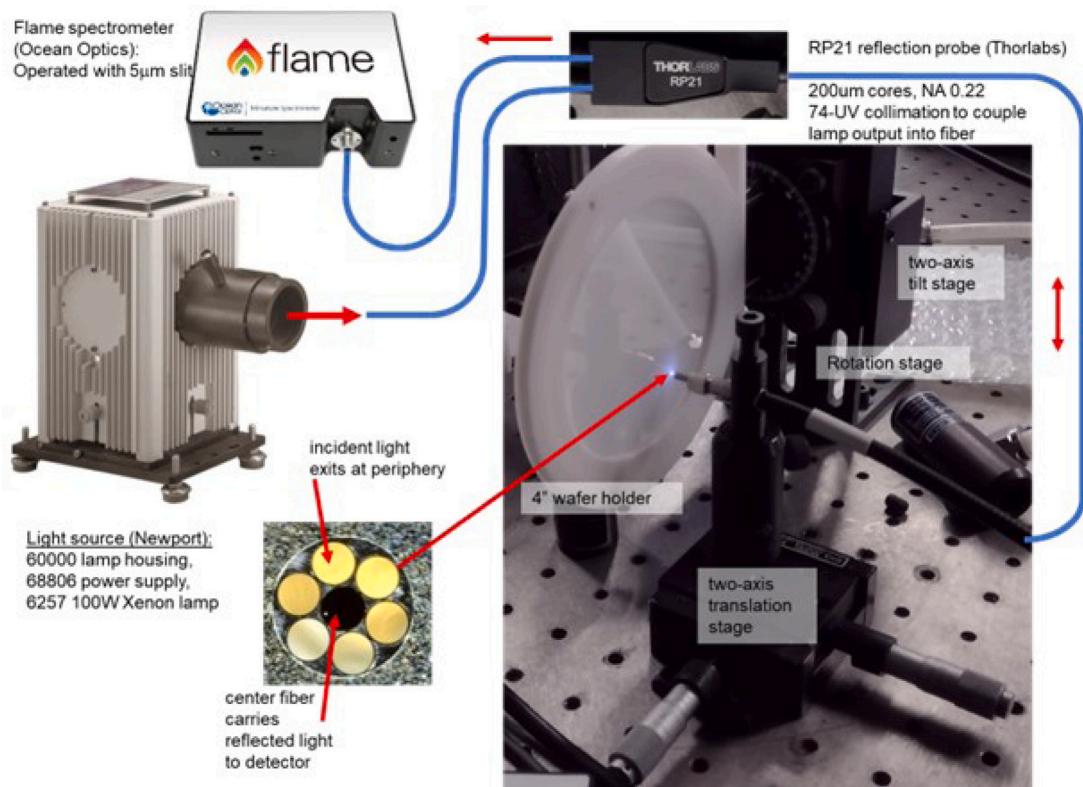


Fig. 6. Reflectance measurement set-up: (a) A reflection probe was used with the reflected light guided in the inner fiber and the illuminating light in the surrounding fibers. The tilt and rotation stages were used for selecting a suitable position on the wafer and for setting the angle of incidence.

types are acceptable if  $A_{QWOT}$  should be limited to 10%. However, the choice for the N-rich materials also limits the refractive index contrast to  $\Delta_c = 0.226$ , while a higher reflectance spectral selectivity can be achieved for the stoichiometric materials, because of  $\Delta_c = 0.280$ . The requirements on  $\Delta_c$  and  $A_{QWOT}$  depend on the specifications of the application and the acceptable complexity of the resulting Bragg reflector design in terms of number of layer pairs.

The optical data is used for the design of a simple 3-layer DBR-alike structure and a more sophisticated 9-layer DBR. The designs are targeting a design wavelength  $\lambda_o = 330$  nm and layers are deposited on silicon wafers. Simulations are performed for the three different material compositions of  $\text{SiN}_x$  for use as high-index layer as defined in Table 1: stoichiometric, slightly N-rich ( $N_{medium}$ ), and highly N-rich. Simulations are based on numerically calculating the system input admittance,  $y_{sys}$ , by multiplication of the characteristic matrices of the different layers in the stack [22]. From  $y_{sys}$  the overall spectral reflectance, transmittance and absorbance can be derived when also considering the free-space input domain and the admittance of the Si substrate,  $y_{Si}$ . The design approach of the DBR taken here is straightforward and involves selecting a layer thickness equal to  $1 \times QWOT$  at  $\lambda_o = 330$  nm and building a stack, with no attention paid to the effect of wavelength dependence of the substrate admittance. It should be noted that a more sophisticated design approach would yield a superior spectral reflectance. However, the priority in this work is on material characterization and the specific spectral transmission of the generic DBR is considered more suitable for that purpose. The simulated spectral responses of a 3-layer H-L-H DBR design are shown in Fig. 4.

The results demonstrate that the straightforward matching to QWOT is inadequate for a practical 3-layer DBR design. The peak reflectance is at a wavelength slightly shorter than 300 nm for  $\text{Si}_3\text{N}_4$  and shifts to a higher peak at a wavelength slightly longer than 300 nm for N-rich  $\text{SiN}_x$ , but remains below  $\lambda_o$ . However, the pronounced spectral shape of the reflectance can be conveniently used for material characterization.

Table 3  
Settings for DBR designs at  $\lambda_o = 330$  nm.

| Symbol                   | Description                     | Stoich | Slightly N-rich | Highly N-rich |
|--------------------------|---------------------------------|--------|-----------------|---------------|
| $n_H = n_{\text{SiN}_x}$ | $\text{SiN}_x$ refractive index | 2.209  | 2.136           | 2.017         |
| $t_{\text{SiN}_x}$       | $\text{SiN}_x$ thickness [nm]   | 37.3   | 38.6            | 40.8          |
| $t_{\text{SiO}_2}$       | $\text{SiO}_2$ thickness [nm]   | 55     | 55              | 55            |

For this reason, combined with the short fabrication sequence, the 3-layer design is used in the analysis presented here.

A comparison of Figs. 4a, 4b and 4c reveals the interplay between transmittance and absorbance, which are both bulk effects. The primary effect of the huge layer absorbance in the spectral range up to about 310 nm is the very small transmittance. This balance changes somewhat with  $x$  in that range, but the increased transmittance with  $x$  is much more significant in the spectral range 310–400 nm. However, also the reflectance, which is in principle a multiple-surface effect at the discontinuities of the index of refraction throughout the stack, is affected by  $x$ . This is because with decreasing  $x$  there is a reduced contribution to interference at the air-DBR surface of a light component that is reflected at a particular  $n_H - n_L$  discontinuity deeper in the stack of layers and, thus, has experienced more absorption along the overall optical path.

The concept can be extended to a 9-layer H-L-H-L-H-L-H-L-H DBR design on a silicon substrate. The simulated spectral response of this Bragg filter for the different  $\text{SiN}_x$  compositions for  $n_H$  considered are shown in Fig. 5. The reduced layer absorption at  $\lambda_o$  for  $\text{SiN}_x$  with  $x$  from stoichiometric to N-rich is evident from the figure. The actual setting of the layer thickness for the different material compositions are summarized in Table 3

### 3. Fabrication and experimental validation

Stacks of alternately  $\text{SiN}_x$  and  $\text{SiO}_2$  layers were deposited by PECVD on 4-inch Si wafers using one of the recipes presented in Table 1. No masking was applied and the entire wafer surface was coated.

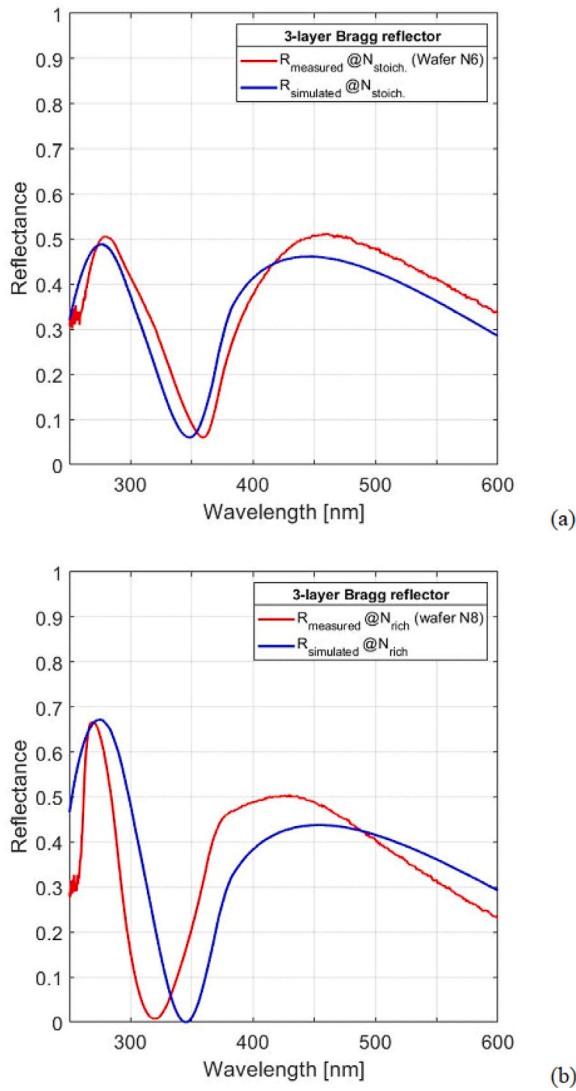


Fig. 7. Measured spectral reflectance for two 3-layer DBR designs: (a) using  $N_{stoich}$  and (b) using  $N_{rich}$ .

Two of the 3-layer H-L-H Bragg reflector designs were fabricated. The first was based on the stoichiometric  $SiN_x$  (identified as wafer N6) and the second on N-rich  $SiN_x$  (wafer N8). In addition only the 9-layer H-L-H-L-H-L-H-L-H design using the N-rich  $SiN_x$  was fabricated (wafer N10). Subsequently, the spectral reflectance was measured using the set-up shown in Fig. 6.

A special multi-fiber probe was used for illuminating the sample and for returning the reflected light. A translation stage was used for selecting a suitable location on the wafer for measurement and for testing uniformity of reflectance over a wafer, while a rotation stage was used to enable adjustment for normal incidence. A 20D10AL.2 UV/visible reference reflector was used for calibration (Newport Corporation). The results of the spectral measurements are shown in Fig. 7. The associated simulated reflectance presented in Section 2.2 is added for enabling a direct assessment of the degree of agreement.

The measured spectral reflectance off the 3-layer DBR on wafer N6 is in qualitative agreement with the simulations. The positions of the measured peaks of reflectance are shifted from 240 nm to 260 nm and from about 450 nm to 460 nm as compared to the values in the simulation.

Comparison of the measured spectral reflectance off N8 and simulations indicate that the magnitude of the shorter-wavelength spectral

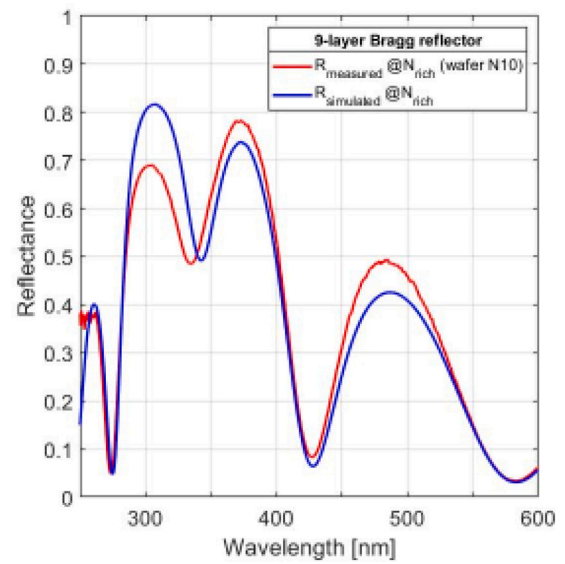


Fig. 8. Measured spectral reflectance for the 9-layer DBR design using  $N_{rich}$ .

reflectance peak does indeed increase with  $x$ . However, also the deviations of the measured spectral position of the peaks and their magnitudes from simulations increase with  $x$ .

Spectral measurements of the 9-layer DBR realized on N10 are presented in Fig. 8, which show reasonable agreement with the simulations, especially with respect to the positions of the peak spectral reflectance. This observation justifies the conclusion that the spectral data on  $n$  is sufficiently robust for use in optical device design.

#### 4. Discussion and conclusions

Demonstrating the usefulness of N-rich  $SiN_x$  for optical design in the near-UV is the primary objective of this work. In Fig. 3b is shown that the lower-wavelength limit of the design window for a  $SiN_x/SiO_2$  filter with acceptable loss in the near-UV shifts from about 450 nm for stoichiometric material to 330 nm for N-rich material. This promise is indeed confirmed in the spectral response of the fabricated 9-layer DBR as presented in Fig. 8. The simulations indicate that the benefit is primarily due to the increased transmittance at the expense of the reduced absorbance, which also improves the spectral reflectance in the near-UV.

The design strategy used here of simply matching  $\lambda_o$  to  $t_{QWOT}$  is a 3-layer device does not result in a reflectance spectrum of practical interest, but rather in a simple test structure for validating and confirming the general expectations, as outlined in Figs. 7a and b. A comparison with the results in Fig. 4 shows reasonable agreement.

Matching  $\lambda_o$  to  $t_{QWOT}$  is a more appropriate approach in the 9-layer DBR design. The spectral position of the peak reflectance in the 9-layer DBR evaluated is in good approximation material independent, as shown in Fig. 5, while the magnitude of peak spectral reflectance increases with  $x$ . The measurements on the 9-layer DBR, as shown in Fig. 8, are in reasonable agreement with the simulations, as shown in Fig. 5c, including the predicted ‘saddle-shaped’ indentation at about 350 nm wavelength for N-rich material. This aspect can be explained by considering the Si optical data. Literature data on crystalline silicon was used and interpolated for obtaining a sufficient spectral resolution for use in simulations, and the data is shown in Fig. 9a [42].

As  $|y_{Si}|$  is proportional to  $|n_{Si}^*|$ , the Si admittance varies significantly over the near-UV part of the spectrum, with peaks at the maximum of  $n_{Si}$  at  $\lambda \sim 380$  nm and at the maximum of  $k_{Si}$  at  $\lambda \sim 280$  nm and a dip at  $\lambda_o \sim 330$  nm in between, which is almost like an spectral signature of the material.



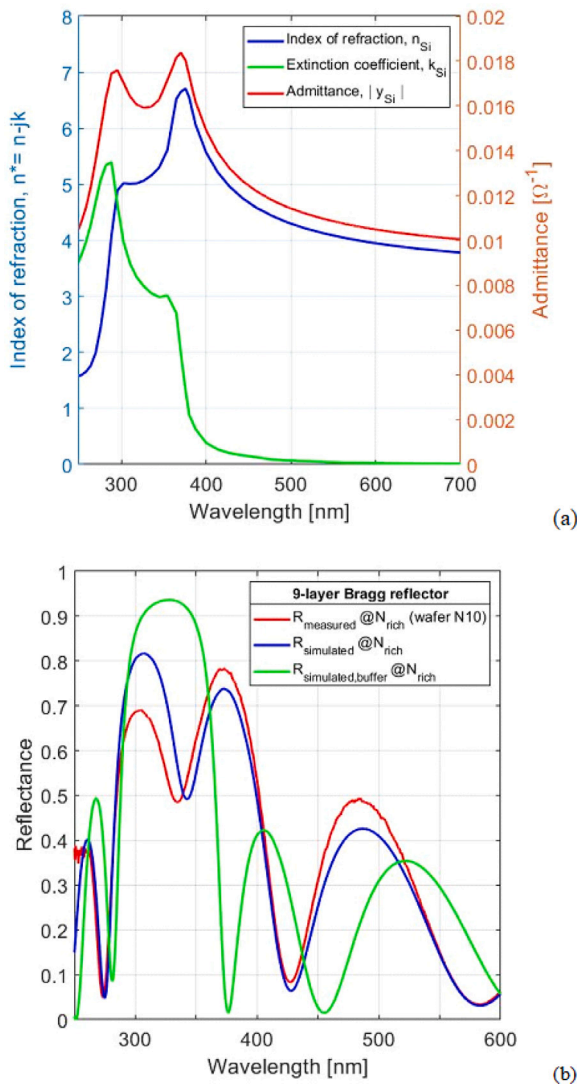


Fig. 9. (a) The spectral dependence of the silicon index of refraction, extinction coefficient and resulting admittance and (b) using a QWOT/2 of  $SiO_2$  buffer layer in between the substrate and the lower  $n_H$  layer for reducing the effect of the Si substrate on the Bragg reflectance for  $n_H = n_{Nrich}$ .

The reduced near-UV layer absorption with increasing  $x$  results in a more-transparent layer material and thus in principle in a high magnitude of the spectral reflectance peak at  $\lambda_o$  of a DBR-design in the near-UV for a high  $x$ . However, as a side effect, also the transfer of the substrate admittance to the surface of incidence is improved, which adversely affects the overall spectral Bragg reflectance at the wavelength range of high spectral substrate admittance. The result is the already mentioned ‘saddle-shaped’ indentation in the DBR spectrum in the near-UV, which deepens with increasing  $x$  (see also the trend from Fig. 5a to 5c). As a consequence the benefit of the improved optical properties of the N-rich material in the near-UV part of the spectrum is reduced. This effect does not appear in the case of a low-loss substrate, as is demonstrated by our initial work on  $SiN_x$  optical devices on sapphire [43].

A solution is to insert a layer of half a QWOT thickness ( $t_{buffer} = t_{QWOT}/2$ ) in  $n_L$  in between the lower  $n_H$  layer and the Si substrate as shown in Fig. 9b. Such a half-QWOT layer is known to effectively buffer the substrate admittance and to suppress the second-order overall reflection in the DBR [22]. The result is a sharper overall spectral reflection with a higher value of the peak reflectance at  $\lambda_o$  and an

extended free spectral range,  $\lambda_{FSR}$ . Fig. 9b shows a peak reflectance  $R_{DBR,max} = 0.936$  at  $\lambda_o = 327$  nm and  $\lambda_{FSR} = 78$  nm. More significantly, the in-band reflectance of the DBR is relatively smooth and remains larger than 90% over the spectral range from 306 nm to 347 nm, which makes this design suitable for fabrication of a LVOF with a coefficient of Finesse,  $F > 4R(1 - R)^{-2} = 360$ . Therefore, a relatively high value for  $F$  can be achieved in the buffered DBR over a large spectral range, which is essential for high spectral selectivity within a relatively large  $\lambda_{FSR}$  and for a high dynamic range (ratio between the peak transmittance and the theoretical minimum of the out-of-band transmittance) of an optical resonator such as the LVOF [22,31].

The design window for optical devices that include layers of stoichiometric  $SiN_x$  is demonstrated to be limited to about 450 nm. This is consistent with literature and has been the reason that  $SiN_x$  is generally not considered for optical design in the near-UV. This work demonstrates that N-rich  $SiN_x$  enables a shift of the lower-wavelength limit of the design window to about 330 nm wavelength. More precisely, from Fig. 3b it can be estimated that the range of PECVD settings for a useful  $SiN_x$  should be such that the proportion of silane in the gas flow is limited to about  $R_{g,max} = 0.1$ . A further reduction of  $R_g$  to a value below 0.076 would, in principle, enable to push the lower wavelength limit of the design window deeper into the UV. However, this ambition would be ultimately constrained by the manufacturing repeatability of the deposition rate and the resulting uncertainties in the composition of the deposited material. The limit is, obviously, depending on the specifics of the equipment used and the acceptable level of uncertainty, but  $R_g \sim 0.04$  with an operating range down to 300 nm wavelength would be realistically achievable. However, the index of refraction,  $n_{SiN_x}$  would also reduce with  $x$  and as a result the index of refraction contrast of a DBR section would reduce, as shown in Fig. 3a. As a consequence the number of  $n_H - n_L$  sections in the DBR for achieving a challenging spectral selectivity would become unpractical for realization in a silicon cleanroom environment.

The assessment of the manufacturability at the wafer level would require the specification of the variation of the  $SiN_x$  optical properties over the wafer, which is not included in this explorative study. However, initial observations indicate a repeatability over a wafer of about 2%, which is in the same order of magnitude as measurement uncertainties, such as the oblique incidence of the probing light beam in the measurement set-up used.

Applications considered for future work are in liquid absorption spectroscopy or biofuel composition measurement [44] and the selective detection of formaldehyde, with a detailed spectral signature in the absorption coefficient in the 300–355 nm band, in the presence of  $NO_2$ , with a gradual increase in spectral absorption coefficient in the range from 250 nm up to wavelengths in the visible spectrum, using UV gas absorption spectroscopy in the 300–360 nm band [45].

#### CRedit authorship contribution statement

**Reinoud F. Wolffenbuttel:** Writing – review & editing, Writing – original draft, Validation, Supervision, Methodology, Investigation, Formal analysis, Conceptualization. **Declan Winship:** Investigation, Conceptualization. **Yutao Qin:** Investigation. **Yogesh Gianchandani:** Writing – review & editing, Supervision, Investigation, Conceptualization. **David Bilby:** Validation, Investigation. **Jaco H. Visser:** Validation, Supervision, Investigation, Funding acquisition.

#### Declaration of competing interest

The authors declare that they have no known competing financial interests or personal relationships that could have appeared to influence the work reported in this paper.

#### Data availability

Data will be made available on request.

## Acknowledgments

Fabrication was carried out at the Lurie Nanofabrication Facility of the University of Michigan and optical characterization at the Ford Center for Research and Advanced Engineering. Financial support for this project was provided in part by a Ford university research project grant (URP), USA, project number 1661.

## References

- [1] C. Yang, J. Pham, Characteristic study of silicon nitride films deposited by LPCVD and PECVD, *Silicon* 10 (2018) 2561–2567.
- [2] P.J. French, P.M. Sarro, R. Mallee, E.J.M. Fakkeldij, R.F. Wolffenbuttel, Optimization of a low-stress silicon nitride process for surface-micromachining applications, *Sensors Actuators A* 58 (1997) 149–157.
- [3] A. Bagolini, A. Picciotto, M. Crivellari, P. Conci, P. Bellutti, PECVD silicon-rich nitride and low stress nitride films mechanical characterization using membrane point load deflection, *J. Micromech. Microeng.* 26 (2016) 025004.
- [4] S. Irmer, K. Alex, J. Daleiden, I. Kommallein, M. Oliveira, F. Römer, A. Tarraf, H. Hillmer, Surface micromachined optical low-cost all-air-gap filters based on stress-optimized Si<sub>3</sub>N<sub>4</sub> layers, *J. Micromech. Microeng.* 15 (2005) 867–872.
- [5] M. Ghaderi, R.F. Wolffenbuttel, Design and fabrication of ultrathin silicon-nitride membranes for use in UV-visible airgap-based MEMS optical filters, *J. Phys. Conf. Ser.* (2016) 757.
- [6] Y. Lin, Z. Yong, X. Luo, S.S. Azadeh, J.C. Mikkelsen, A. Sharma, H. Chen, J.C.C. Mak, P.G.Q. Lo, W.D. Sacher, K.S. Poon, Monolithically integrated, broadband, high-efficiency silicon nitride-on-silicon waveguide photodetectors in a visible-light integrated photonics platform, *Nature Commun.* 13 (2022) 6362.
- [7] J.A. Smith, H. Francis, G. Navickaitė, M.J. Strain, SiN foundry platform for high performance visible light integrated photonics, *Opt. Mater. Express* 13 (2023) 458–468.
- [8] C. Xiang, W. Jin, J.E. Bowers, Silicon nitride passive and active photonic integrated circuits: trends and prospects, *Photonics Res.* 10 (2022) A82–A96.
- [9] S. Romero-García, F. Merget, F. Zhong, H. Finkelstein, J. Witzens, Silicon nitride CMOS-compatible platform for integrated photonics applications at visible wavelengths, *Opt. Express* 21 (2013) 14036–14046.
- [10] C.G.H. Roeloffzen, M. Hoekman, E.J. Klein, L.S. Wevers, R.B. Timens, et al., Low-loss Si<sub>3</sub>N<sub>4</sub> TriPleX optical waveguides: Technology and applications overview, *IEEE J. Sel. Top. Quant. Electron.* 24 (4) (2018) 1–21.
- [11] P. Muñoz, G. Micó, L.A. Bru, D. Pastor, D. Pérez, J.D. Doménech, J. Fernández, R. Baños, B. Gargallo, R. Alemany, A.M. Sánchez, J.M. Cirera, R. Mas, C. Domínguez, Silicon nitride photonic integration platforms for visible, near-infrared and mid-infrared applications, *MDPI Sensors* 17 (9) (2017) 2088.
- [12] H. Son, Y.J. Lee, S. Jung, K. Jang, J. Kim, J. Cho, J. Heo, B.S. Kim, Memory characteristics of MNOS capacitors with various energy band gaps of silicon nitride, *J. Korean Phys. Soc.* 54 (4) (2009) 1492–1495.
- [13] H. Chariñ, A. Slaoui, J.P. Stoquert, H. Chaib, A. Hannour, Opto-structural properties of Silicon Nitride thin films deposited by ECR-PECVD, *World J. Condens. Matter Phys.* 6 (2016) 7–16.
- [14] C.J. Krücker, A. Fülöp, Z. Ye, P.A. Andrekson, V. Torres-Company, Optical bandgap engineering in nonlinear silicon nitride waveguides, *Opt. Express* 25 (2017) 15370–15380.
- [15] S. Garcia, D. Bravo, M. Fernandez, I. Martil, F.J. López, Role of oxygen on the dangling bond configuration of low oxygen content SiN<sub>x</sub>:H films deposited at room temperature, *Appl. Phys. Lett.* 67 (22) (1995) 3263–3265.
- [16] D.N. Wright, E.S. Marstein, A. Rognmo, A. Holt, Plasma-enhanced chemical vapour-deposited silicon nitride films; the effect of annealing on optical properties and etch rates, *Sol. Energy Mater. Sol. Cells* 92 (2008) 1091–1098.
- [17] T. Makino, Composition and structure control by source gas ratio in LPCVD SiN<sub>x</sub>, *J. Electrochem. Soc.* 130 (1983) 450–455.
- [18] H. Mäckel, R. Lüdemann, Detailed study of the composition of hydrogenated SiN<sub>x</sub> layers for high-quality silicon surface passivation, *J. Appl. Phys.* 92 (5) (2002) 2602–2609.
- [19] J.F. Lelièvre, E. Fourmond, A. Kaminski, O. Palais, D. Ballutaud, M. Lemiti, Study of the composition of hydrogenated silicon nitride SiN<sub>x</sub>:H for efficient surface and bulk passivation of silicon, *J. Sol. Energy Mater. Solar Cells* 93 (8) (2009) 1281–1289.
- [20] F. Ay, A. Aydinly, Comparative investigation of hydrogen bonding in silicon based PECVD grown dielectrics for optical waveguides, *Opt. Mater.* 26 (2004) 33–46.
- [21] L. Asinovsky, U.F. Shen, T. Yamaguchi, Characterization of the optical properties of PECVD SiN films using ellipsometry and reflectometry, *Thin Solid Films* 313–314 (1998) 198–204.
- [22] H.A. Macleod, *Thin-Film Optical Filters*, Institute of Physics Publishing, 2001.
- [23] E.M. Esposito, L.V. Mercaldo, P. Delli Veneri, L. Lancellotti, C. Privato, Annealing effects on PECVD-grown Si-rich a:SiN<sub>x</sub> thin films, *Energy Procedia* 2 (2010) 159–164.
- [24] A. Emadi, H. Wu, G. de Graaf, R.F. Wolffenbuttel, Design and implementation of a sub-nm resolution microspectrometer based on a Linear-Variable Optical Filter, *Opt. Express* 20 (2012) 489–507.
- [25] F.L. Martínez, M. Toledano-Luque, J.J. Gandía, J. Cárabe, W. Bohne, J. Röhrich, E. Strub, I. Mártil, Optical properties and structure of HfO<sub>2</sub> thin films grown by high pressure reactive sputtering, *J. Phys. D Appl. Phys.* 40 (2007) 5256–5265.
- [26] S.F. Pellicori, C.L. Martinez, UV optical properties of thin-film oxide layers deposited by different processes, *Appl. Optics* 50 (28) (2011) 5559–5566.
- [27] R. Thielsch, A. Gatto, J. Heber, N. Kaiser, A comparative study of the UV optical and structural properties of SiO<sub>2</sub>, Al<sub>2</sub>O<sub>3</sub>, and HfO<sub>2</sub> single layers deposited by reactive evaporation, ion-assisted deposition and plasma ion-assisted deposition, *Thin Solid Films* 410 (1–2) (2002) 86–93.
- [28] L. Gao, F. Lemarchand, M. Lequime, Exploitation of multiple incidences spectrometric measurements for thin film reverse engineering, *Opt. Express* 20 (14) (2012) 15734–15751.
- [29] F. Bridou, M. Cuniot-Ponsard, J.M. Desvignes, M. Richter, U. Kroth, A. Gottwald, Experimental determination of optical constants of MgF<sub>2</sub> and AlF<sub>3</sub> thin films in the vacuum ultra-violet wavelength region (60–124 nm) and its application to optical designs, *Opt. Commun.* 283 (7) (2010) 1351–1358.
- [30] K. Iwahori, M. Furuta, Y. Taki, T. Yamamura, A. Tanaka, Optical properties of fluoride thin films deposited by RF magnetron sputtering, *Appl. Opt.* 45 (19) (2006) 4598–4602.
- [31] M. Bischoff, D. Gäbler, N. Kaiser, A. Chuvilin, U. Kaiser, A. Tünnermann, Optical and structural properties of LaF<sub>3</sub> thin films, *Appl. Opt.* 47 (13) (2008) 157–161.
- [32] A. Emadi, H. Wu, G. de Graaf, P. Enoksson, J.H. Correia, R.F. Wolffenbuttel, Linear variable optical filter-based ultraviolet microspectrometer, *Appl. Opt.* 51 (19) (2012) 4308–4315.
- [33] R. Korde, J. Geist, Stable, high quantum efficiency, UV-enhanced silicon photodiodes by arsenic diffusion, *Solid-State Electron.* 30 (1) (1987) 89–92.
- [34] Y. Aoyagi, Y. Fujihara, M. Murata, H. Shike, R. Kuroda, S. Sugawa, A CMOS image sensor with dual pixel reset voltage for high accuracy ultraviolet light absorption spectral imaging, *Japan. J. Appl. Phys.* 58 (2019).
- [35] GSI-PECVD <https://Inf-wiki.eecs.umich.edu/wiki/GSI-PECVD>,
- [36] CompleteEASE Training Series <https://www.jawoollam.com/resources/videos/completeease-training-series>,
- [37] D.I. Patel, D. Shah, J.N. Hilfiker, M.R. Linford, A tutorial on spectroscopic ellipsometry (SE); 5. Using the Tauc-Lorentz and Cody-Lorentz models to describe the absorption features of amorphous silicon (a-Si), *Vacuum Technol. Coat.* (2019) 34–37.
- [38] D. Amans, S. Callard, A. Gagnaire, J. Joseph, G. Ledoux, F. Huisken, Ellipsometric study of silicon nanocrystal optical constants, *J. Appl. Phys.* 93 (7) (2003) 4173–4179.
- [39] L.V. Rodriguez-de Marcos, J.I. Larruquert, Analytic optical-constant model derived from Tauc-Lorentz and Urbach tail, *Opt. Express* 24 (25) (2016) 28561–28572.
- [40] O. Pluchery, J.M. Costantini, Infrared spectroscopy characterization of 3C-SiC epitaxial layers on silicon, *J. Phys. D: Appl. Phys.* 45 (2012) 495101.
- [41] Z. Hameiri, N. Borojevic, L. Mai, N. Nandakumar, K. Kim, S. Winderbaum, Should the refractive index at 633 nm be used to characterize silicon nitride films? in: *IEEE 43<sup>rd</sup> Photovoltaic Specialists Conference, PVSC, IEEE, 2016*, pp. 2900–2904.
- [42] D.E. Aspnes, A.A. Studna, Dielectric functions and optical parameters of Si, Ge, GaP, GaAs, GaSb, InP, InAs, and InSb from 1.5 to 6.0 eV, *Phys. Rev. B* 27 (1983) 985–1009.
- [43] R.F. Wolffenbuttel, D. Winship, D. Bilby, J.H. Visser, Y. Qin, Y. Gianchandani, SiN<sub>x</sub>/SiO<sub>2</sub>-based Fabry-Perot interferometer on sapphire for near-UV optical gas sensing of formaldehyde in air, *MDPI Sensors* 24 (11) (2024) 3597.
- [44] L.M. Middelburg, G. de Graaf, A. Bossche, J. Bastemeijer, M. Ghaderi, F.S. Wolffenbuttel, J.H. Visser, R. Soltis, R.F. Wolffenbuttel, Multi-domain spectroscopy for composition measurement of water-containing bio-ethanol fuel, *Fuel Process. Technol.* 167 (2017) 127–135.
- [45] J.J. Davenport, J. Hodgkinson, J.R. Saffell, R.P. Tatam, A measurement strategy for non-dispersive ultra-violet detection of formaldehyde in indoor air: spectral analysis and interferent gases, *Meas. Sci. Technol.* 27 (2016) 015802.